Array of virtual Frisch-grid CZT detectors with common cathode readout and pulse-height correction

A. E. Bolotnikov[a], G. S. Camarda[a], Y. Cui[a], S. U. Egarievwe[b], P. M. Fochuk[a,c], M. Fuerstnau[a] , R. Gul[a], A. Hossain[a], F. Jones[a] , K. Kim[a], O. V. Kopach[a,c], R. Taggart[a], G. Yang[a], Z. Ye[a], L. Xu[a,d], and R. B. James[a]

[a]Brookhaven National Laboratory, Upton, NY, USA

[b]Alabama A&M University, Huntsville, Al, USA

[c]Chernivtsi National University, Chernivtsi, Ukraine

[d]Northwestern Polytechnic University, Xi'an, Shaanxi, China.

ABSTRACT

We present our new results from testing 15-mm-long virtual Frisch-grid CdZnTe detectors with a common-cathode readout for correcting pulse-height distortions. The array employs parallelepiped-shaped CdZnTe (CZT) detectors of a large geometrical aspect ratio, with two planar contacts on the top and bottom surfaces (anode and cathode) and an additional shielding electrode on the crystal's sides to create the virtual Frisch-grid effect. We optimized the geometry of the device and improved its spectral response. We found that reducing to 5 mm the length of the shielding electrode placed next to the anode had no adverse effects on the device's performance. At the same time, this allowed corrections for electron loss by reading the cathode signals to obtain depth information.

Keywords: CdZnTe detectors, virtual Frisch-grid detectors, crystal defects

1. INTRODUCTION

Development of room temperature gamma-ray CdZnTe (CZT) detectors, currently underway in the National Laboratories, universities, and industry, is vital for many applications including medical imaging, astronomy, and homeland security [1]. CZT detectors operate as single-type carrier (electrons), meaning that the devices' geometrical parameters and contacts configurations should be chosen so to minimize the contribution of uncollected holes, whose effect on output signals depends on the location of interaction points. In this work, we investigated the performance of 6x6x15 mm^3 virtual Frisch-grid detectors [2-8] assembled in 4x4 detector arrays with a common cathode-readout for correcting pulse-height and rejecting incomplete charge-collection events. This type of detector provides excellent energy resolution, <1.5% FWHM at 662 keV, and large effective areas. They offer a robust, low-cost approach to making the large-area detecting planes that potentially can substitute for more advanced but more expensive 3D devices [9] in applications with slightly relaxed requirements for position- and energy-resolution. In addition, rejecting the incomplete charge collection (ICC) events allows one to use imperfect crystals from less expensive material.

Although the 3D devices operating in a time-projection-chamber mode represent the most advanced technology in CZT detectors, they are not practical today for making large-effective area instruments because of the low availability and high cost of big crystals, ~20x20x15 mm^3, required by this approach. In contrast, the thick crystals, up to 20 mm, but with small cross-sectional area, ~6x6 mm^2, used in virtual Frisch-grid detectors are fabricated from relatively thin, 7 mm, CZT wafers that impart better screening and greater flexibility in cutting before making the actual devices. Each

Hard X-Ray, Gamma-Ray, and Neutron Detector Physics XII, edited by Arnold Burger, Larry A. Franks, Ralph B. James,
Proc. of SPIE Vol. 7805, 780504 · © 2010 SPIE · CCC code: 0277-786X/10/$18 · doi: 10.1117/12.861775

bar, working as an independent detector, potentially can attain nearly intrinsic energy-resolution and high detection-efficiency. A 4x4 array of virtual Frisch-grid detectors has a similar area and volume as a 3D detector. Both types of detectors offer correction for charge loss, imaging capability, and background rejection. The special resolution provided by the array (determined by the cross-sectional area of the bars) is suitable for using such arrays as detection planes in coded-aperture telescopes. As we demonstrated previously [6-8], an energy resolution between 0.8- and 1.5% -FWHM at 662 keV can be achieved with regular spectroscopic-grade CZT material; this is about twice the resolution obtained for 3D devices, 0.6%, made from the pre-selected crystals. This resolution is adequate for resolving most gamma-ray spectra. Because of its particular geometry, the achievable active volume of the 6x6x15 mm^3 virtual Frisch-grid detector is ~75% of its total volume, assuming that material is free from major defects, compared with ~90% possible with 2.5-mm pitch 3D devices. In reality, both characteristics, viz., detection efficiency and energy resolution, are determined by the quality of the CZT crystal used to fabricate the devices. Based on our results from testing over 50 virtual Frisch-grid detectors, we estimate that the average effective volume of the 6x6x15 mm^3 devices made with material of average quality is 50-70% of their total volumes. However, making larger area arrays of inexpensive crystals can easily offset such losses in efficiency.

The important performance characteristic of a CZT detector is its sensitivity, which is in inverse proportion to the effective area and square root of the energy resolution. If we compare virtual Frisch-grid- and 3D-detectors, the latter gains a factor of 1.4 because of their twofold better energy resolution. Nevertheless, making larger virtual Frisch-grid detectors can compensate for this drawback.

The design of a virtual Frisch-grid detector relies on using a large geometrical-aspect ratio, parallelepiped-shaped (bar) crystals with the cathode and anode electrodes, respectively, deposited on the top- and bottom-surfaces and an additional shielding electrode placed on a crystal's side to create the virtual Frisch-grid effect. We fabricate such devices by wrapping or coating the sides of a crystal with a thin layer of an insulating film, followed by a layer of aluminum- or copper-foil. Using long CZT crystals with a high geometrical aspect ratio is a key requirement for achieving high-energy resolution and a high peak-to-Compton ratio. However, in thick devices, electron trapping by defects can be severe and must be corrected to retain high spectral-resolution. Implementing a cathode-readout scheme assures this by allowing us firstly to correct for electron trapping, and secondly, to reject events interacting near the anode and contributing to the background. Previously, we demonstrated that, in 15-mm long detectors, a wide area near the cathode can be left uncovered by the shield without lowering the effectiveness of shielding the anode [8]. Furthermore, assembling the arrays in which the cathodes of several detectors, i.e., the 4x4 modules, are connected together enhances the shielding effect. This design should efficiently shield the anode whilst allowing us to read out the cathode signals required for correcting charge losses due to electron trapping.

Carrier trapping results in incomplete charge collection (ICC) that inhibits the detector's efficiency and spectral response. A straightforward solution to this problem is to use selected CZT crystals with low concentrations of defects. Although this approach is acceptable for small detectors, it is too expensive when using large, >5x10 cm^3, crystals. Today, the yield of large crystals with acceptable levels of defects is low, while their cost is high. Another solution for this problem is to recognize and reject (or veto) ICC events. Such a rejection algorithm is possible for any single-polarity carrier device in which the amplitudes of the signals are read out from the cathode and anode, and the ratios of the signals are correlated with the electron drift time. Rejecting ICC events does not entail additional loss of photo-efficiency, but may significantly improve the spectral response (energy resolution and peak-to-Compton ratio), and enhance the sensitivity of devices fabricated from crystals with relaxed quality requirements. Such crystals typically are those now available from vendors.

In this paper, we describe the results from testing of the 15-mm-long virtual Frisch-grid detectors with signal-readout from both the cathode and anode. We related the measured detector's responses to the material-characterization data obtained via IR transmission microscopy and X-ray diffraction topography. The goal of our work was to demonstrate performance, and identify the factors limiting the energy resolution of the new virtual Frisch-grid detectors. Our next step will be to fabricate an array of 6x6x15 mm^3 detectors and test it with the readout electronics based on the new ASIC for pixel detectors recently developed at BNL's Instrumentation Division. If successful, we planned to make and test an array consisting of 20-mm-long detectors that would increase their efficiency, spectral performance, and ability to measure high-energy photons (> 1 MeV).

2. EXPERIMENTAL SETUP

We tested over 50 6x6x15 mm^3 virtual Frisch-grid detectors fabricated from two 7-mm thick CZT wafers from two different ingots. The wafers possessed a similar resistivity of >3x10^{10} Ohm-cm, and an electron $\mu\tau$-product of >7x10^{-3} cm^2/V, as measured by the vendor. Later, our more accurate measurements of the $\mu\tau$-products yielded a typical value of >2x10^{-2} cm^2/V.

First, we characterized the wafers using IR transmission microscopy to measure the concentrations and size distributions of Te inclusions by taking "in depth" images of 1.1x1.5 mm^2 areas at different locations [10]. The concentration of Te inclusions was the same within a factor of ~2 over the wafers' areas, except for the regions containing decorated grain boundaries. Then, we chemically etched the wafers to identify areas free from grain boundaries and twins, from which we cut the detectors. Unfortunately, this procedure did not guarantee 100% success in selecting good crystals, because neither IR microscopy nor surface etching identified the dislocation-related defects, such as walls of dislocation, cellular structures, low-angle boundaries, and sub-grain boundaries, all of which turned out to be very critical in determining the devices' performances. Using the White X-Ray Beam Diffraction Topography (WXDT) technique, we found that it was practically impossible to avoid wafers containing large concentrations of sub-grain boundaries and dislocation bands distributed over their entire area. Although these types of defects can be very detrimental to the device's performance we purposely ignored them, at least for now, so that we could better understand their roles and to test our algorithm to minimize their effects. Afterwards, we sent the wafers back to the vendor for making 6x6x15 mm^3 detectors with two planar Pt contacts.

The design of the virtual Frisch-grid detector array with a common cathode, and a procedure for fabricating it are described in Ref. [9]. We tested the as-received crystals for leakage current, and then encapsulated them in ultra-thin polyester shells. To complete the device, we placed 5.0-5.5 mm-wide shielding electrodes made of aluminum foil near the anode electrodes, as shown in Fig. 1(a); as we demonstrated previously, this is optimal for 6x6x15 mm^3 crystals [9].

During the testing, we put the detector inside a special holder with two BNC connectors (Fig. 1b). This arrangement allowed us to apply a high-voltage bias on the cathode and to read the signals from both the cathode and anode. The test sources were sited about ~7 cm above the detector to keep the count rate sufficiently low to eliminate overlapping pulses. A 2000-V bias was applied to the cathode.

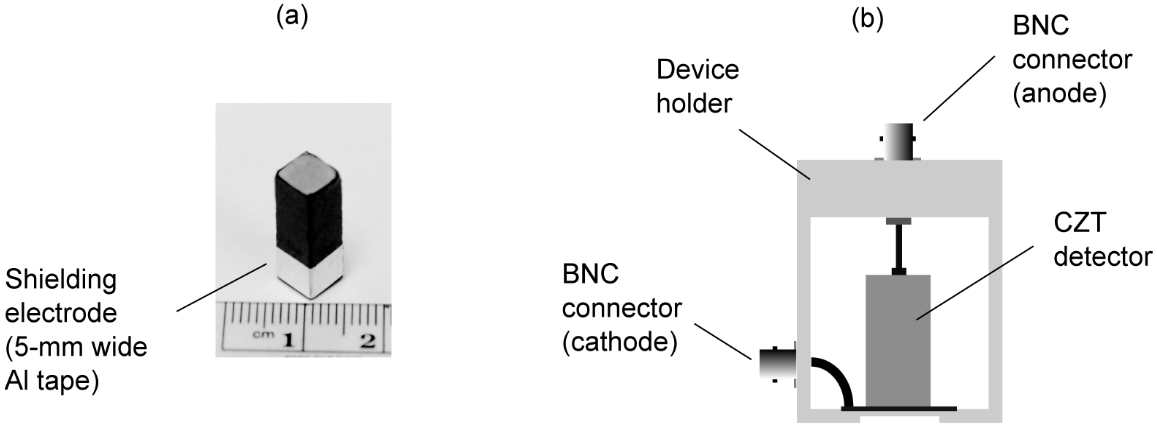

Fig. 1. (a) A photograph of a 6x6x15 cm^3 virtual Frisch-grid detector encapsulated in a 100-μm thin polyester shell with a 5-mm wide shielding electrode; (b) Schematic of the device holder with two BNC connectors.

We employed a LeCroy Waverunner to digitize and record the output signals (waveforms) read out from the anode and cathode with eV-Microelectronics charge-sensitive preamplifiers (eV-5093). We applied a digital-pulse analysis described elsewhere [11] to evaluate the pulse-height spectra and the dependencies of the signals' amplitudes versus the electrons' drift-times. Fig. 2 shows typical signals captured from the cathode- and anode-contact. The horizontal dashed line defines a threshold for the cathode signal, while the vertical dashed ones define the event-accruing time (left) and the electron arrival time at the anode (right). The drift time is determined as the time between these two moments. We evaluated the amplitudes of the anode- and cathode-signals by averaging the corresponding top, flat portion of the pulses over ~500 ns after the baseline subtraction [11]. A set of at least 20,000 waveforms was gathered, and used to evaluate the dependence on the amplitudes of the output signals measured from the anode and cathode versus the drift-time and pulse-height spectra.

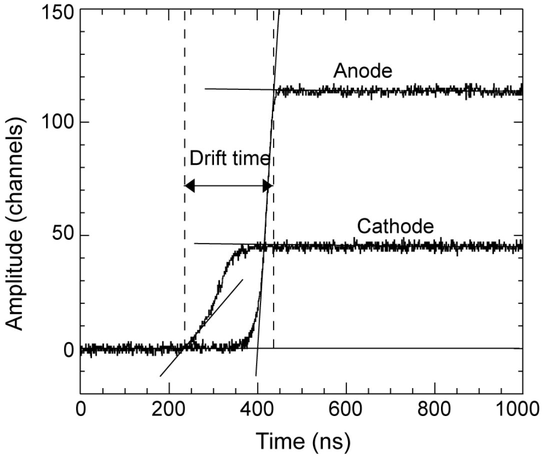

Fig. 2. Typical signals captured from the cathode and anode. Two vertical ones define the interaction time (left), and electron arrival time at the anode (right). The drift time is determined as the interval between these two moments.

3. RESULTS AND DISCUSSION

3.1 Device testing

Previously [9], we carried out a series of measurements of pulse-height spectra and the dependences of the amplitudes of the anode and cathode signals versus the electron drift time (correlation curves) from a 6x6x15 mm^3 virtual Frisch-grid detector equipped with shielding electrodes of different widths. We demonstrated that we can reduce the width of the shielding electrode so that it covers only ~5 mm of the detector's length without affecting the device's performance.

Out of 50 fabricated detectors, twelve had excessively high leakage currents (likely related to the network of sub-grain boundaries network that provided conductive pathways between the cathode and the anode), and could not be used. Fig. 3 plots the typical dependences of the anode- and cathode-signals versus the drift time measured for a representative detector with a 5-mm wide shielding electrode. Since the drift times correspond to the distances of the electron clouds from the anode, these dependencies represent correlations between the output signals and the interaction depth. Each dot in these distributions represents an event that the device detected. The full-energy absorption events are concentrated along the curved lines whose shapes are determined by changes of the weighting potential inside the device, and by electron loss due to trapping. For the anode signals, over most of the device (except for the region near the anode) these two effects, approximated by linear functions with opposite slopes, partially compensate for each other, generating a nearly flat response. As is evident, the response rapidly declines below a certain distance from the anode. Analogous to the classic gas-ionization chamber, in the Frisch-grid this distance can be marked as a location of the virtual Frisch-grid (shown as a vertical dashed line). For the cathode signals, a close-to-linearly rising function in the distance interval between the virtual Frisch-grid and the cathode approximates the signals' dependence. The slope of the anode's dependence is used to correct charge losses due to electron trapping. For each interaction, events triggered by the cathode, the anode- and cathode-signals are processed to evaluate the corresponding pulse-heights and the drift times that, in turn, are used to generate and correct the pulse-height spectra. Fig. 4 depicts the pulse-height spectra generated after each step of pulse processing from three representative detectors: (a) good, (b) average, and (c) poor.

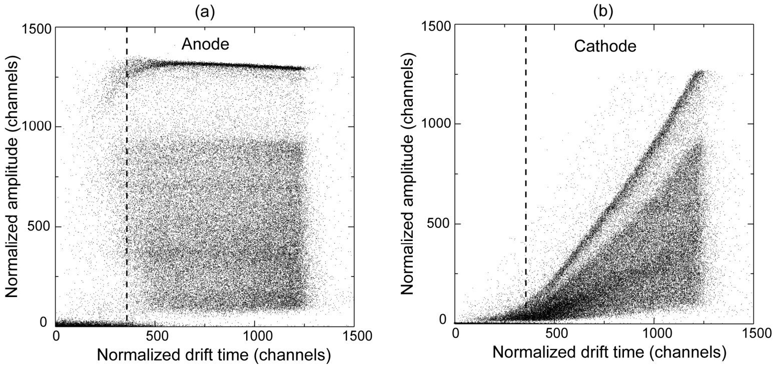

Fig. 3. Dependences of the anode (a) and cathode (b) signals vs. the drift time (correlation curves) measured for a good 6x6x15 mm^3 virtual Frisch-grid detector with a 5-mm wide shielding electrode placed near the anode.

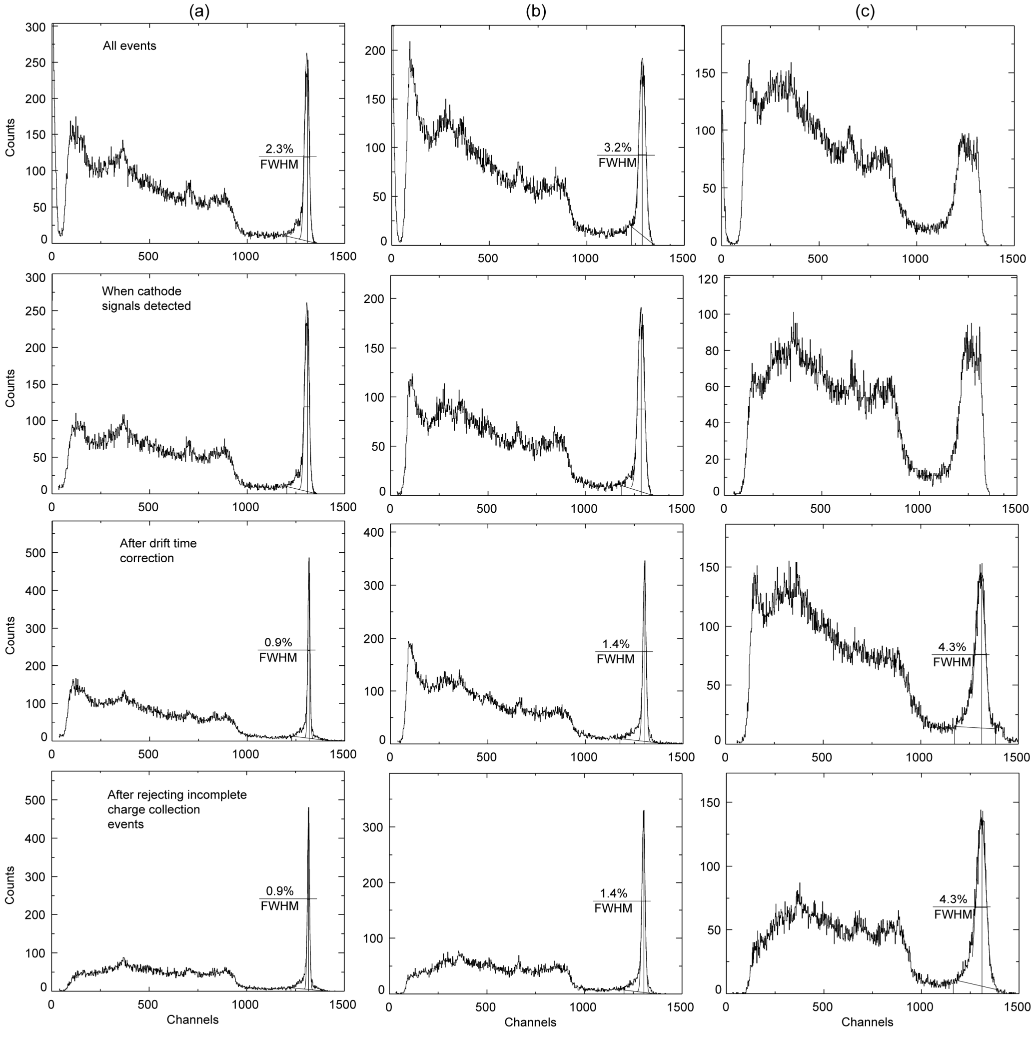

Fig. 4. Pulse-height spectra generated after each step of pulse processing from three representative detectors: (a) Good, (b) average; and, (c) poor.

The top row in Fig. 4 represents the original all-events spectra (regardless of the cathode signals) measured from the detectors. The spectra in the second row contain only those events for which the cathode signals exceeded one sigma above the noise level. As is evident, these spectra have notably smaller low-energy continuums, mostly populated by the events interacting near the anode, while the photopeaks remain intact. The third row shows the spectra after applying the drift-time correction that uses the slopes of the correlation curves like that shown in Fig. 3(a). Clearly, such corrections improve the devices' energy resolution without events losses. Finally, the last row (bottom) shows the corrected spectra after rejecting the incomplete charge-collection events. This procedure cleaned up the spectra by removing them from the continuum while retaining the true Compton scattering events and all original photopeak events. We emphasize that the virtual Frisch-grid detector offers a way to veto the majority of the ICC events resulting from these defects. We have illustrated above (Fig. 4) the application of the rejection technique for spectral responses generated by the ^{137}Cs source.

To demonstrate that this technique is applicable to improving the pulse-height spectra generated by multiple gamma lines, we used a ^{133}Ba source to illuminate the detector. Fig. 5 shows the spectra generated after each step of pulse processing for the good detector.

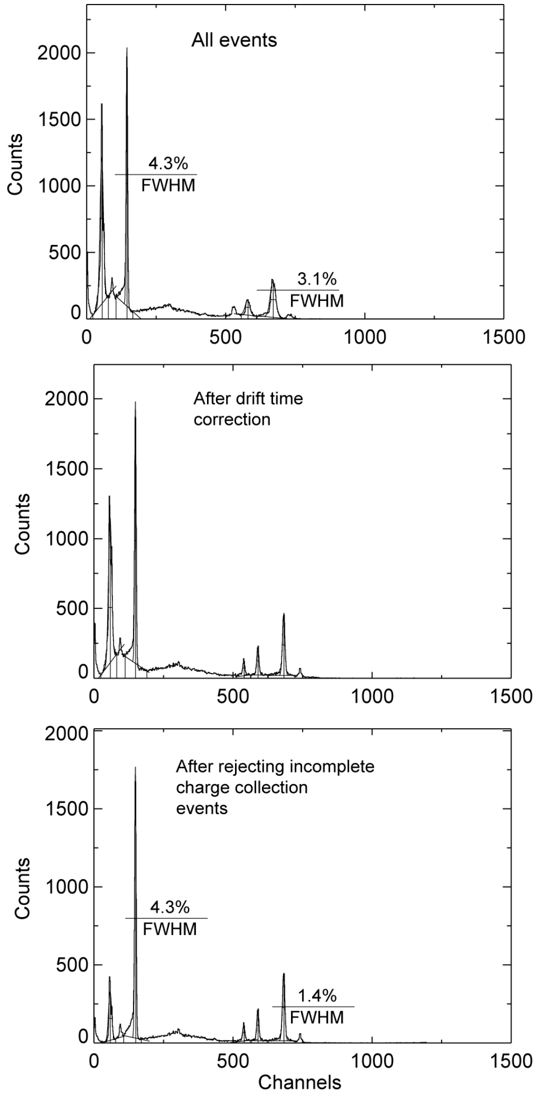

Fig. 5. Pulse-height spectra generated after each step of pulse processing from a good detector illuminated with a ^{133}Ba source.

3.2 Roles of Te inclusions

As illustrated in Fig. 6, the crystal from wafer #1 had notably smaller Te inclusions than did wafer #2. Thus, we expected that they would degrade the performance of detectors fabricated from the second wafer. Fig. 7 shows the scatter plots of energy resolution versus inclusion concentration (with diameters greater than 3 μm) measured for the detectors from both wafers. As seen, we found no correlation between concentration of Te inclusions and energy resolution for detectors fabricated from wafer #1. For wafer #2, the data points located at the bottom of the distribution indeed follow a straight line, in agreement with the predictions given in Ref. [12]. From this, we conclude that the peak broadening due to Te inclusions in the detectors fabricated from wafer #1 (with small inclusions) is less than 0.8%. For detectors fabricated from wafer #2 (with its large inclusions), their photopeak broadening increases with the concentration of inclusions. The data points located above the line indicated that there are other dominating defects. We show next that subgrain boundaries and dislocations bands are more critical defects degrading the detectors' responses.

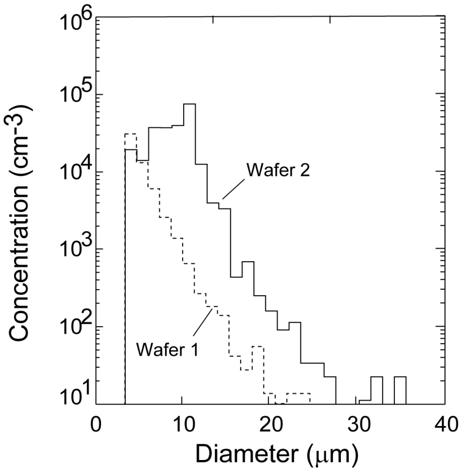

Fig. 6. Typical size distributions of Te inclusions found in the samples cut from two wafers.

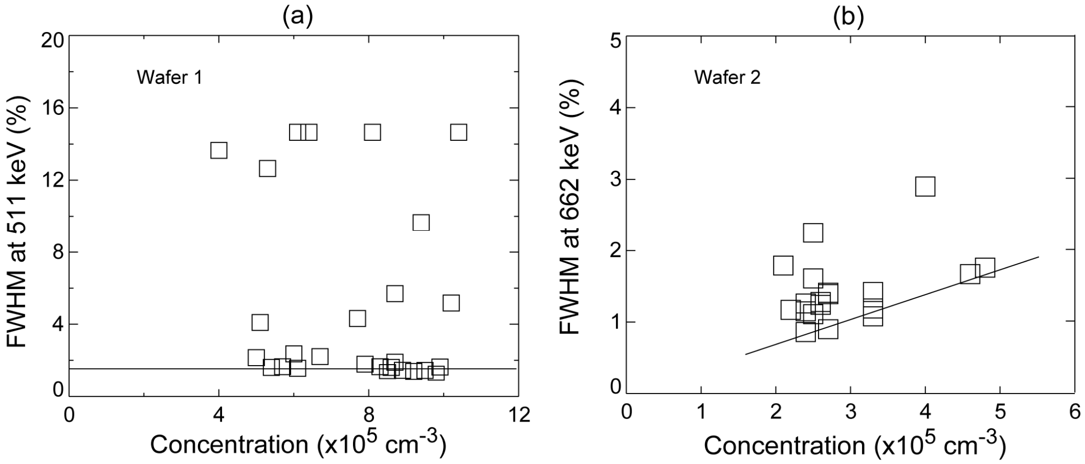

Fig. 7. Energy resolution: (a) and (b) correlation between energy resolution and concentration of Te inclusions with diameters greater than 3 μm measured for the crystals cut from wafers #1 and #2, correspondingly.

3.3 Roles of subgrain boundaries and walls of dislocations

Our previous studies indicated the importance of the dislocation-related defects present in high-quality commercial material, e.g., from the vendors eV-Microelectronics, ICx Radiation, Yinnel Tech, and Redlen, viz., boundaries and cellular structures, consisting of arranged dislocations of different densities. The differences between subgrain boundaries, low-and high-angle boundaries, diffuse boundaries, and walls of dislocations primarily are related to their geometrical sizes and dislocation densities. Fig. 5 shows examples of subgrain boundaries revealed by WXDT (a), and the walls of dislocations exposed by surface etching (b).

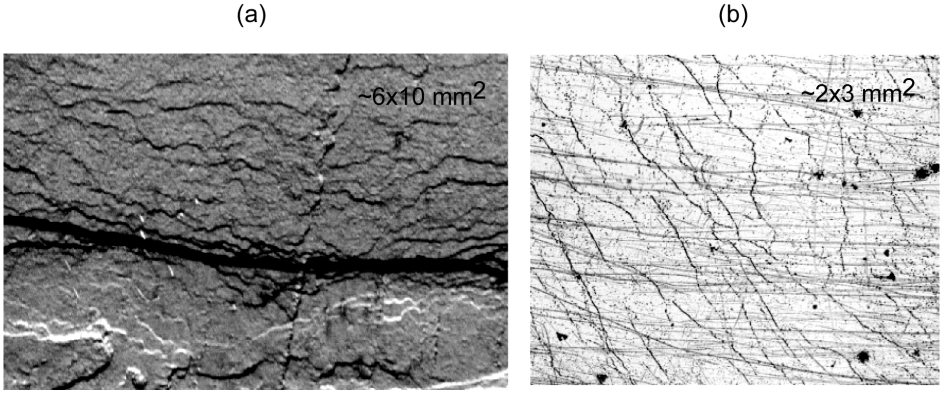

Fig. 5. Subgrain boundaries: (a) WXDT image of a large subgrain boundary along with a network of small dislocation bands; (b) image of the etched surface revealing walls of dislocations.

Dislocations are known to accumulate high concentrations of electron traps and affect the local electric field and, consequently, the drift paths of electron clouds. In the large-aspect ratio devices, like virtual Frisch-grid detectors, the curved electron paths can reach the side surfaces of a crystal before the anode, resulting in signal losses. Regardless of the nature of these defects, they can be associated with macroscopic regions filled with traps; however, unlike point defects, such regions are not distributed uniformly over devices' volumes. The continuous charge losses caused by point defects correlate with the electrons' drift times, so that we can correct for them. The inhomogeneous distribution of traps results in random charge losses that are not correctable. Depending on the amount of lost charge, it can affect the spectral responses in two ways. If the amount of charge lost after an electron cloud encounters a defect is small, it is likely that these defects would cause broadening of the photopeak, since such small variations in the charge loss would accumulate with drift distances. These losses typically are associated with small Te inclusions, 3 µm, and a low density of dislocation boundaries. Conversely, if a significant amount of charge is trapped, this will cause the photopeak events to move toward the Compton continuum, meaning that resolution will stay intact, while the photopeak efficiency will decrease. Such charge losses are associated with a high density of dislocation boundaries and big Te inclusions, >50 µm. Clearly, in thin crystals, <2 mm, in which the broadenings of electron clouds due to diffusion are small, efficiency will be affected most. In thick devices, small inclusions and dislocations likely will entail deterioration in the energy resolution. In other words, a low density of dislocation boundaries and Te inclusions are more critical in long, >10 mm, devices. We mentioned that the rejection algorithm entails no extra loss of photopeak efficiency to that caused by the bad regions of the crystal.

3.4. Factors limiting the energy resolution

The virtual Frisch-grid detectors potentially can provide the statistic-limited resolution. However, the electronic noise is inherently higher in these types of detectors compared to pixel devices because of the anode's higher capacitance. The best energy resolution (after correcting for charge loss) that we measured with 6x6x15 mm^3 virtual Frisch-grid detectors was 0.8% FWHM at 662 keV for room-temperature operation. After subtracting the contribution of electronic noise, ~3.5 keV, we estimated a value of 0.6%, which is very close to the statistical limit. The averaged energy resolution measured for all detectors was ~1.3%. We attribute the degradation of the energy resolution in many of the detectors we tested to defects in CZT crystals. We describe them in their order of the importance.

Point defects (native and impurities) can trap up to 20% of the charge in long-drift time detectors. However, because their spatial distributions usually are described by slowly changing functions, charge losses can be corrected, and energy resolution can be recovered to its intrinsic value.

The effects of Te inclusions depend on their sizes and concentration. Small inclusions, <3 μm, behave similarly to point defects, but big inclusions, >10 μm, entail significant fluctuations in the collected charge. As we discussed, it is very likely that such inclusions set the low limit on the energy resolution in detectors fabricated from the second wafer.

Dislocation-related defects are the most detrimental to the devices' spectral responses. These defects are linear dislocations and dislocations arranged in two- and three-dimensional structures (i.e., walls of dislocations, low-angle and subgrain boundaries, and cellular- and mosaic-structures). Dislocations accumulate impurities and secondary phases (Te inclusions). Depending on the dislocations' density and orientation, they trap both the significant- and small-fractions of the electrons from the charge clouds. They also affect the trajectories of local electric fields and electron-cloud drifts. Interplay between these defects may result in broadening of photopeaks, and increases in the continuum in the majority of our detectors. Figs. 9-13 show examples of pulse-height spectra (original and after correction and ICC rejection) measured with several representative detectors fabricated from the CZT crystals with different contents of the dislocation-related defects, as revealed with WXDT. These figures also illustrate that, in many cases, the pulse-height spectra can be significantly improved by using the drift-time correction- and ICC rejection-techniques. The original (all events) and corrected spectra (after both such modifications) are shown on the top and at bottom, correspondingly. The image on the left is a WXDT topograph taken for the two orthogonal sides of the detector.

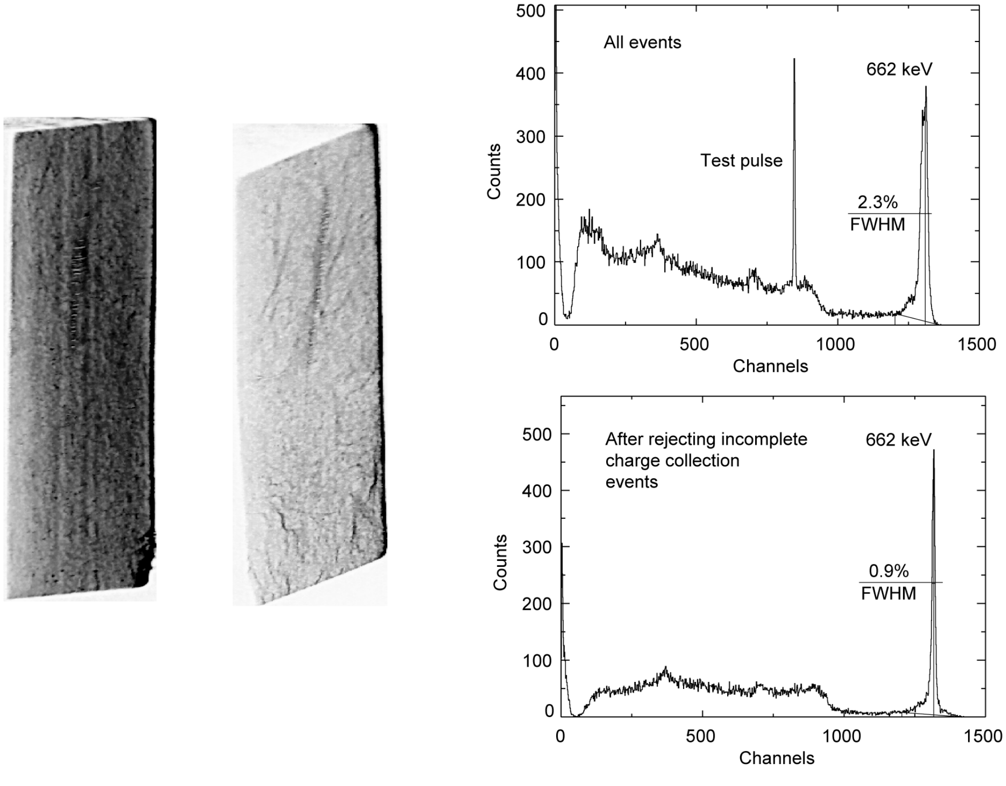

Fig. 9. Pulse-height spectra before (top) and after (bottom) corrections taken with a "good" detector. The WXDT topograph shows a small content of the subgrain boundaries that correlates with a small increase of the continuum. The peak width (%FWHM) is likely to be governed by the effects of Te inclusions.

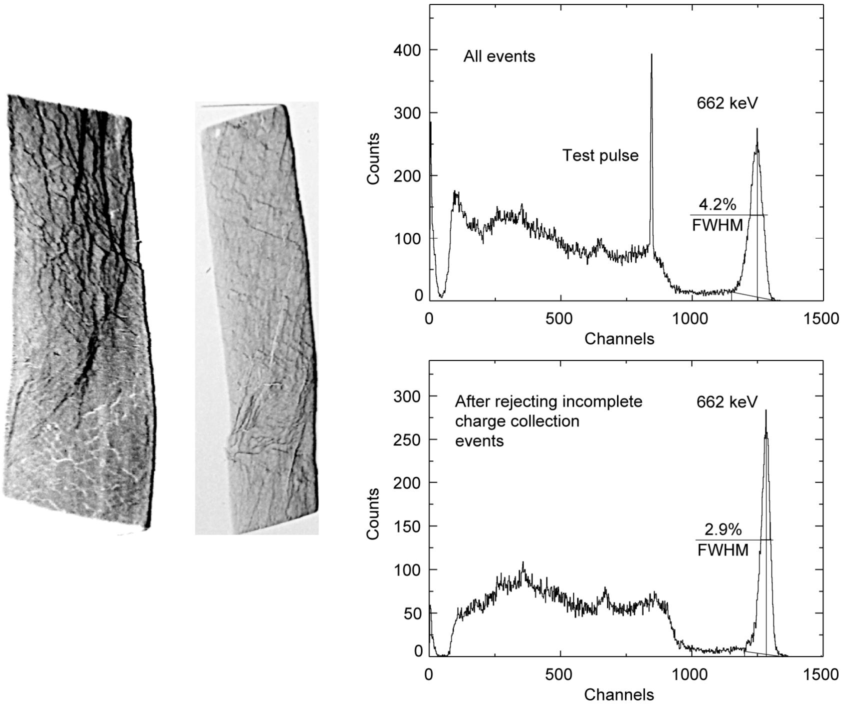

Fig. 10. Pulse-height spectra before (top) and after (bottom) corrections taken with a "bad" detector. The WXDT topograph shows a small content of the subgrain boundaries that correlates with a small increase of the continuum. The peak width (%FWHM) is likely to be governed by the effects of dislocations and subgrain boundaries.

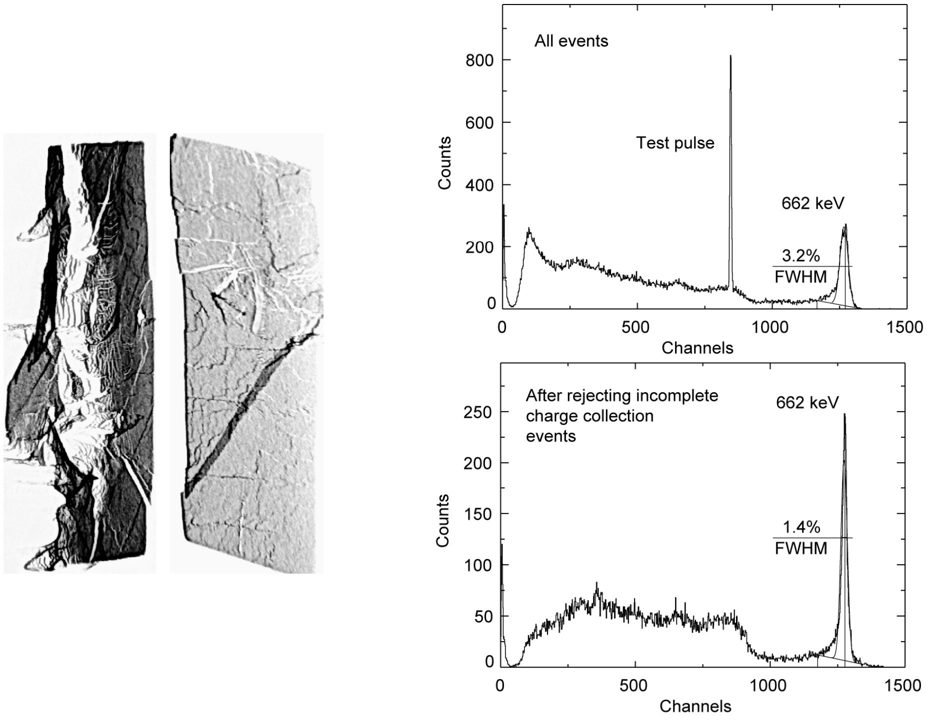

Fig. 11. Same caption as Fig. 10. We note here how rejecting ICC events improves the pulse-height spectrum (bottom).

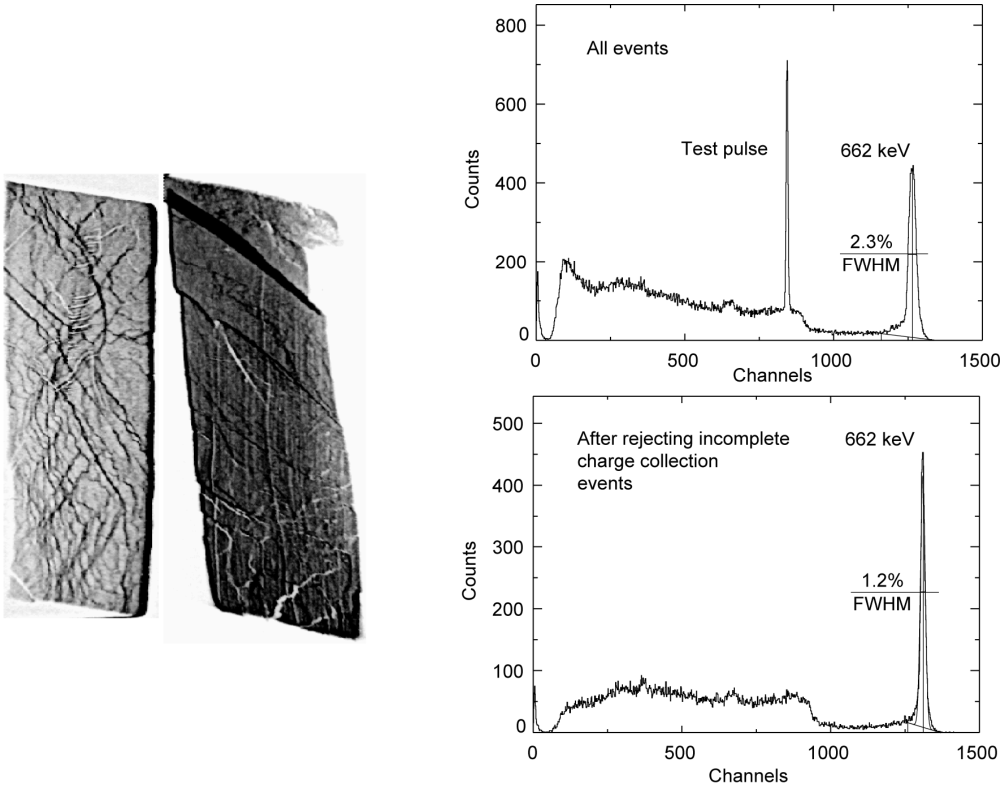

Fig. 12. Same caption as Fig. 10. We note here how rejecting ICC events improves the pulse-height spectrum (bottom).

4. CONCLUSIONS

We fabricated and tested the virtual Frisch-grid detectors and explored the possibility of using the cathode signals for electron charge-loss correction. For the majority of the crystals, we achieved an energy resolution ranging from 0.8% to 2% FWHM at 662 keV after this correction. We demonstrated that rejecting incomplete charge-collection events improves the pulse-height spectra, thereby allowing the use of crystals with defects that are less expensive than good ones, and also have high availability.

The device's performance was primary limited by dislocation-related defects: The walls of dislocations, low-angle and sub-grain boundaries, and, sometimes, cellular structures. These defects are located only by X-ray diffraction topography. To overcome these problems, more uniform ingots must be grown.

ACKNOWLEDGMENT

This work was supported by U.S. Department of Energy, Office of Nonproliferation Research and Development, NA-22 and Defense Threat Reduction Agency. The manuscript has been authored by Brookhaven Science Associates, LLC under Contract No. DE-AC02-98CH1-886 with the U.S. Department of Energy. The United States Government retains, and the publisher, by accepting the article for publication, acknowledges, a world-wide license to publish or reproduce the published form of this manuscript, or allow others to do so, for the United States Government purposes.

REFERENCES

[1] G. Knoll, *Radiation Detection and Measurement,* 3rd ed. New York: Wiley 2000.

[2] A. E. Bolotnikov, N. M. Abdul-Jabbar, S. Babalola, G. S. Camarda, Y. Cui, A. Hossain, E. Jackson, H. Jackson, J. R. James, A. L. Luryi, and R. B. James, "Optimization of virtual Frisch-grid CdZnTe detector designs for imaging and spectroscopy of gamma rays", Invited Paper, in Proceedings of SPIE Hard X-Ray and Gamma-Ray Detector Physics VIII, Vol. 6702, edited by L. A. Franks, A. Burger, R. B. James, H. B. Barber, F. P. Doty, and H. Roehrig (SPIE, Bellingham, WA, 2007).

[3] D.S. McGregor and R.A. Rojeski, U.S. Patent 6,175,120.

[4] G. Montemont, M. Arques, L. Verger, and J. Rustique, "A Capacitive Frisch Grid Structure for CdZnTe Detectors", IEEE Trans. Nucl. Sci., Vol. 48, pp. 278-281, 2001.

[5] A. E. Bolotnikov, G. S. Camarda, G. A. Carini, M. Fiederle, L. Li, D. S. McGregor, W. McNeil, G. W. Wright, and R. B. James, "Performance Characteristics of Frisch-Ring CdZnTe Detectors", IEEE Trans. on Nucl. Sci., Vol. 53 (2), pp. 607-614, 2006.

[6] A. E. Bolotnikov, N. M. Abdul-Jabbar, S. Babalola, G. S. Camarda, Y. Cui, A. Hossain, E. Jackson, H. Jackson, J. R. James, A. L. Luryi, and R. B. James, "Optimization of virtual Frisch-grid CdZnTe detector designs for imaging and spectroscopy of gamma rays", Invited Paper, in Proceedings of SPIE Hard X-Ray and Gamma-Ray Detector Physics IX, Vol. 6702, edited by R. B. James, A. Burger, L. A. Franks, (SPIE, San Diego, CA, 2007), pp. 670603-1 – 670603-14.

[7] A. E. Bolotnikov, S. Babalola, G. S. Camarda, Y. Cui, S. U. Egarievwe P. M. Fochuk, R. Hawrami, A. Hossain, J. R. James, I. J. Nakonechnyj, Ge Yang, and R. B. James, "Spectral responses of virtual Frisch-grid CdZnTe detectors and their relation to IR microscopy and X-ray diffraction topography data", in SPIE Conference on Hard X-Ray, Gamma-Ray and Neutron Detector Physics X, Vol. 7079, edited by A. Burger, L. Franks and R. B. James (SPIE, Bellingham, WA, 2008), pp. 707903-1.

[8] J. K. Polack, M. Hirt, J. Sturgess, N. D. Sferrazza, A. E. Bolotnikov, S. Babalola, G. S. Camarda, Y. Cui, S. U. Egarievwe, P. M. Fochuk, R. Gul, A. Hossain, K. Kim, O. V. Kopach, L. Marchini, G. Yang, L. Xu, and R. B. James, "Variation of electric shielding on virtual Frisch-grid detectors", Nucl. Instr. Meth. A621, pp. 424-430, 2010.

[9] F. Zhang, Z. He, D. Xu, G. F. Knoll, D. K. Wehe, and J. E. Berry, "Improved resolution for 3D position sensitive CdZnTe spectrometers," IEEE Trans. Nucl. Sci., Vol. 51, pp. 2427-2431, 2004.

[10] A. E. Bolotnikov, S. Babalola, G. S. Camarda, Y. Cui, S. U. Egarievwe, R. Hawrami, A. Hossain, G. Yang, and R. B. James, "Te Inclusions in CZT Detectors: New Method for Correcting Their Adverse Effects", IEEE Trans. on Nucl. Sci. 57, pp. 910-919, (2010).

[11] A. E. Bolotnikov, G. S. Camarda, G. A. Carini, M. Fiederle, L. Li, G. W. Wright, and R. B. James, "Performance Studies of CdZnTe Detector by Using a Pulse-Shape Analysis", Proceedings of SPIE Hard X-Ray and Gamma-Ray Detector Physics VII, edited by R. B. James, L. A. Franks, and A. Burger (SPIE, San Diego, CA, 2005), 59200K-1 – 59200K-12.

[12] A. E. Bolotnikov, N. M. Abdul-Jabber, O. S. Babalola, G. S. Camarda, Y. Cui, A. M. Hossain, E. M. Jackson, H. C. Jackson, J. A. James, K. T. Kohman, A. L. Luryi and R. B. James, "Effects of Te inclusions on the performance of CdZnTe radiation detectors", IEEE Trans. on Nucl. Sci. 51, No. 5, 2757-2764 (2008).